

Full Spectrum Modeling of At-Sensor Spectral Radiance Variability Due to Surface Variability¹

John P. Kerekes

Chester F. Carlson Center for Imaging Science
Rochester Institute of Technology
Rochester, New York, USA
kerekes@cis.rit.edu

Jerrold E. Baum

Lincoln Laboratory
Massachusetts Institute of Technology
Lexington, Massachusetts, USA
jbaum@ll.mit.edu

Abstract— In support of hyperspectral sensor system design and parameter tradeoff investigations, an analytical end-to-end remote sensing system performance forecasting model has been extended to cover the visible and near infrared through longwave infrared portion of the optical spectrum (0.4 to 14 μm). The model takes statistical descriptions of surface spectral reflectances and temperature variations in a scene and propagates them through the effects of the atmosphere, the sensor, and processing transformations. A resultant system performance metric is then calculated.

This paper presents the theory for analytically transforming surface statistics to at-sensor spectral radiance statistics for a downward-looking hyperspectral sensor observing both reflected sunlight and thermally emitted radiation. Comparisons of the model's predictions with measurements from an airborne hyperspectral sensor are presented. An example is included to show the model's utility in understanding the magnitude of full spectrum radiance components.

Keywords-spectral imaging; full spectrum modeling

I. INTRODUCTION

Hyperspectral imaging (HSI) systems operating in the reflective solar portion of the optical spectrum (0.4 to 2.5 μm) have demonstrated utility in a variety of applications, ranging from environmental monitoring [1] to subpixel object detection [2]. Extending their operation to cover the full optical spectrum (0.4 to 14 μm) offers the hope of day/night capability and additional applications for hyperspectral sensing using spectral features in the midwave and longwave infrared.

Previously, an end-to-end hyperspectral remote sensing system model has been developed for the solar reflective regime using an analytical framework [3] that built on earlier work [4]. This model, known as Forecasting and Analysis of Spectroradiometric System Performance (FASSP), has been used for sensitivity studies and requirements analysis for systems operating in the reflective solar portion of the spectrum. The work described in this present paper extends the scene portion of the model to the full optical spectrum.

II. ANALYTICAL END-TO-END SYSTEM MODEL

The underlying premises of the model are 1) that the various surface classes and subclasses of interest can be represented by first- and second-order spectral statistics and 2)

¹This work was sponsored by the Department of Defense under Air Force contract F19628-00-C-0002. Opinions, interpretations, conclusions, and recommendations are those of the author and not necessarily endorsed by the United States Government.

that the effects of various processes in the end-to-end spectral imaging system can be modeled as transformations and functions of those statistics. The end-to-end system includes the scene, the sensor, and the processing algorithms that produce a data product.

The model is driven by a user-specified input set of system parameter settings that define the end-to-end scenario, including the scene classes, atmospheric state, sensor characteristics, and processing algorithms. Our previous work [3] described in detail the equations that propagate the statistics through the end-to-end model to obtain a performance metric for the reflective solar part of the spectrum. An upcoming paper [5] describes the extension of the model to the full spectrum. This paper focuses on the extension of the scene radiance sub-model to the combined reflected and emitted case.

III. FULL SPECTRUM SCENE MODEL

The FAASP scene radiance model considers a scene to consist of one, or more, background classes and one target class which may be a linear mixture of target component classes (subclasses). The target is usually considered to be subpixel, or at most, to occupy a single pixel. The statistics for each class, or subclass, include the mean temperature \bar{T} , the temperature variance σ_T^2 , the mean spectral reflectance $\bar{\rho}_\lambda$, and the full spectral reflectance covariance matrix Σ_ρ . The following paragraphs describe how these surface statistics are transformed into at-sensor radiance statistics.

The model for the at-sensor spectral radiance has five terms, as shown in (1). The first two terms represent the solar radiance contributions, while the last three describe the thermally emitted radiance components.

$$L_{At-Sensor} = \frac{1}{\pi} [E_S + E_{DS}] \rho \tau + L_P(\rho_{adj}) \text{ reflected sunlight} \quad (1) \\ + L_B(T)[1 - \rho] \tau + \frac{1}{\pi} E_{DT} \rho \tau + L_U \text{ emitted thermal}$$

Where,

$L_{At-Sensor}$ spectral radiance received by the downward looking sensor,

E_S	solar spectral irradiance incident on surface from direct transmission through atmosphere,
E_{DS}	diffuse atmospherically scattered solar spectral irradiance incident on surface,
ρ	spectral hemispherical reflectance factor for location on surface within sensor's instantaneous field of view (IFOV),
τ	atmospheric transmittance for path from the surface to the sensor,
$L_P(\rho_{adj})$	path scattered solar spectral radiance incident at sensor including the contribution from surface interactions outside the sensor IFOV,
$L_B(T)$	surface emitted spectral radiance from a black body at temperature T ,
E_{DT}	downwelling atmospheric thermally emitted spectral irradiance incident on surface,
L_U	upwelling atmospheric thermally emitted spectral radiance incident at sensor.

In our model, the surface reflectance ρ and surface temperature T are assumed to be uncorrelated random parameters. All other environmental scene parameters (atmospheric profile, etc.) are assumed to be deterministic with user-specified values.

By combining terms equation (1) can be written as

$$L_{At-Sensor} = L_D \rho \tau + L_B(T)[1-\rho]\tau + L_P(\rho_{adj}) + L_U \quad (2)$$

where L_D is the total downwelling (solar direct and diffuse + atmospheric thermal) radiance.

The object of interest, or target, may be composed of M distinct materials (or subclasses). The observed radiance from the object is the weighted linear combination of the radiance from each material. Each material m occupies some area fraction a_m ($\sum_{m=1}^M a_m = 1$) of the total sensor IFOV, or pixel. The resulting observed spectral radiance is computed as the area weighted sum of terms from (2) as shown in (3).

$$L_{AS} = \sum_{m=1}^M L_D \rho_m \tau + \sum_{m=1}^M L_B(T_m)[1-\rho_m]\tau + L_P(\rho_{adj}) + L_U \quad (3)$$

To compute the mean spectral radiance of the target pixel, equation (3) is used directly by substituting the mean values for ρ , T , and ρ_{adj} .

The at-sensor radiance spectral covariance matrix for the pixel of interest can be derived [5] as shown in equation (4).

$$\begin{aligned} \Sigma_{At-Sensor} = & \mathbb{T} \left[\sum_{m=1}^M a_m^2 \{ \Lambda_{\sigma_{L_{Bm}}} \Sigma_{\rho_m} \Lambda_{\sigma_{L_{Bm}}} + \Lambda_{\bar{L}_{Bm}} \Sigma_{\rho_m} \Lambda_{\bar{L}_{Bm}} + \right. \\ & \Lambda_{1-\bar{\rho}_m} \Sigma_{L_{Bm}} \Lambda_{1-\bar{\rho}_m} + \Lambda_{L_D} \Sigma_{\rho_m} \Lambda_{L_D} - (\Lambda_{L_D} \Sigma_{\rho_m} \Lambda_{\bar{L}_{Bm}} + \\ & \left. \Lambda_{\bar{L}_{Bm}} \Sigma_{\rho_m} \Lambda_{L_D}) \} \right] \mathbb{T} + (\Lambda_{L_{P1}} - \Lambda_{L_{P0}}) \Sigma_{\rho_{adj}} (\Lambda_{L_{P1}} - \Lambda_{L_{P0}}) \end{aligned} \quad (4)$$

Where,

- \mathbb{T} diagonal matrix of surface-to-sensor atmospheric transmittance,
- $\Lambda_{\sigma_{L_B}}$ diagonal matrix of surface emitted spectral radiance standard deviation with each entry $\sigma_{L_B} = \sigma_T \partial B / \partial T$ for $T = \bar{T}$, where σ_T is the surface temperature standard deviation and $\partial B / \partial T$ is the derivative of the Planck radiance function,
- Σ_{ρ} spectral reflectance covariance matrix,
- $\Lambda_{\bar{L}_B}$ diagonal matrix of mean Planck spectral radiance emitted by the surface (black body) at temperature \bar{T} ,
- Σ_{L_B} spectral covariance of surface emitted blackbody spectral radiance ($= \Lambda_{\sigma_L} [1] \Lambda_{\sigma_L}$, where $[1]$ is a $K \times K$ matrix of ones),
- $\Lambda_{1-\bar{\rho}}$ diagonal matrix of 1 - mean surface reflectance,
- Λ_{L_D} diagonal matrix of downwelling spectral radiance.
- $\Lambda_{L_{P\alpha}}$ diagonal matrix of path scattered spectral radiance for a surface albedo of α .

The various components are computed using the Air Force Research Laboratory's MODTRAN radiative transfer code [6] and the Planck radiance equation.

Each N background classes is defined to occupy a fraction b_n ($\sum_{n=1}^N b_n = 1$) of the total scene. The background scene average reflectance $\bar{\rho}_{adj}$ is then computed as shown in equation (5).

$$\bar{\rho}_{adj} = \sum_{n=1}^N b_n \bar{\rho}_n \quad (5)$$

The composite scene average background (adjacent) reflectance covariance matrix $\Sigma_{\rho_{adj}}$ is computed as shown in equation (6). Note that since it is computed by using samples of reflectances from the various background classes, the composite covariance is a simple linear weighting of the individual covariances Σ_{ρ_n} .

$$\Sigma_{\rho_{adj}} = \sum_{n=1}^N b_n \Sigma_{\rho_n} \quad (6)$$

This adjacency model assumes the scene is of the same scale as atmospheric particle scattering. The adjacency effect ranges from hundreds of meters to kilometers [7]. This is typically the scale of a scene analyzed with our model.

IV. VALIDATION

Comprehensively validating the scene radiance model would require a data set with known reflectance and temperature statistics for a scene observed by an imaging spectrometer covering the full spectrum. Since such a data set

was not readily available, we demonstrate the ability of the model to represent the radiance statistics in a manner consistent with observations.

Two experiments follow. First, in the LWIR spectral region, we compare the mean spectral radiance and radiance variability statistics predicted by the model to observations of airborne data under reasonable assumptions for the surface statistics. The second experiment is a Monte Carlo simulation of a complex scene with a multiclass target to confirm the analytical derivation for the full spectrum model radiance covariance.

A. Comparison of Airborne LWIR Data and Model Predictions

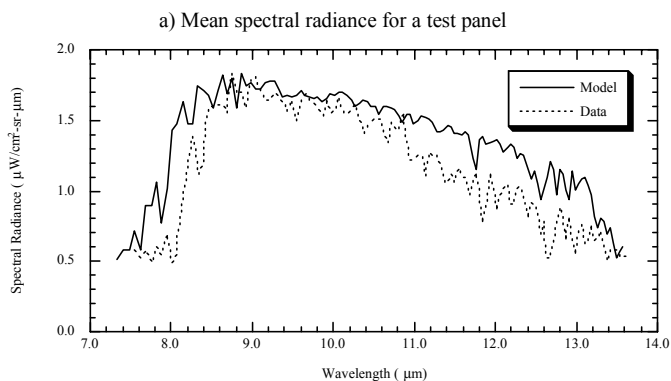
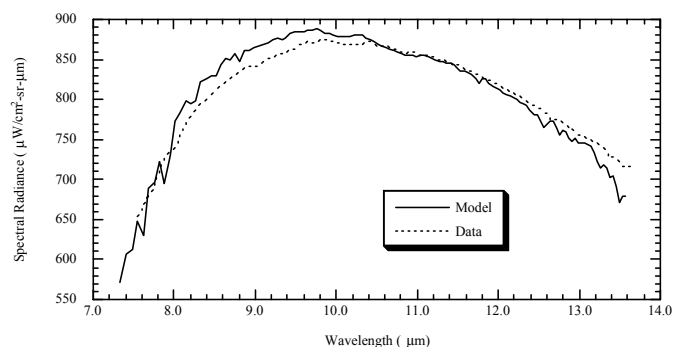
The model predictions were compared to airborne LWIR hyperspectral data collected by the SEBASS [8] instrument on 27 June 1997 at the Department of Energy Atmospheric Radiation Measurements (ARM) site near Lamont, Oklahoma. The scene consisted of wheat fields, pasture, and an area where several test panels were deployed.

The measured data and model predictions were compared in two ways. First, for one of the test panels, the average at-sensor spectral radiance was computed from the data and compared to the model's prediction. Second, over a relatively uniform region of the pasture, the variability (standard deviation) of the at-sensor spectral radiance was compared to that predicted by the model.

1) *Mean Spectral Radiance Comparison.* The measured mean spectral radiance was calculated by averaging the data from nine pixels centered on a calibration panel. To predict the mean spectral radiance, ground measurements of the panel's emissivity and estimates of the scene parameters were input to the model. The comparison is shown in Figure 1a. The match between model prediction and data is within 5%. Differences may be explained by errors in the absolute radiometric calibration of the sensor and by differences between the model atmosphere and the real atmosphere at the time of the data collection.

2) *Spectral Radiance Variability Comparison.* The standard deviation of the measured calibrated spectral radiance was calculated for one hundred pixels of a relatively homogenous area of pasture. For the model, because no accurate emissivity spectra of the pasture were available, a constant greybody mean emissivity of 0.99 was assumed. The variability of the pasture emissivity was represented with a standard deviation of 0.001.

Figure 1b shows that the variability in the sensor data and that predicted by the model have similar overall shapes and magnitudes, but with differences of up to 30-40%. Many of the same atmospheric features are present in both the measured data and the model prediction, but also there are some shifts seen in their peaks that may be due to spectral calibration errors in the data. While the relative differences are large, the absolute error ($< 0.3 \mu\text{W}/\text{cm}^2\text{-sr}\cdot\mu\text{m}$) is quite small.



b) Spectral radiance standard deviation for an area over the pasture

Figure 1. Comparison of calibrated airborne spectral radiance from the SEBASS sensor with model predicted radiance using similar conditions.

B. Simulated Multiclass Full Spectrum Data

To test the multiclass full spectrum model of the propagation of surface statistics to at-sensor radiance statistics, we generated simulated at-sensor radiance data with known atmospheric conditions, target and background abundances, and surface reflectance/temperature statistics. Statistics of the simulated data were then compared to the statistics predicted by the analytical model.

We selected three wavelengths (one each from the visible, midwave infrared, and longwave infrared regions) to span the spectrum and have a multidimensional case. The atmospheric transmittances and spectral radiances were generated by a sample run of MODTRAN.

200,000 samples of simulated at-sensor radiances were generated. A radiance sample from each surface material subclass was calculated and weighted together as in equation (3) using a random temperature (Gaussian distributed), a random path scattered radiance (Gaussian distributed), and a random surface reflectance factor (uniformly distributed).

Table I shows, for the three wavelengths, the at-sensor radiance statistics for the Monte Carlo simulation compared to those predicted by the model. As can be seen, the analytical model propagates the spectral mean, variability, and correlation through the illumination and atmospheric effects in a manner quite similar to the Monte Carlo simulation. This result provides confidence in the model derivation.

TABLE I. COMPARISON BETWEEN SIMULATED EMPIRICAL AND ANALYTICAL MODEL

Parameter	VNIR	MWIR	LWIR
Mean spectral radiance ($W/m^2-\mu m-sr$)			
Monte Carlo Simulation	63.4	0.843	9.59
Analytical Model	63.4	0.842	9.59
Standard deviation of spectral radiance ($W/m^2-\mu m-sr$)			
Monte Carlo Simulation	3.15	0.020	0.130
Analytical Model	3.16	0.021	0.131
Correlation coefficient			
Monte Carlo Simulation	0.254	-0.309	0.610
Analytical Model	0.269	-0.290	0.609

V. EXAMPLE ANALYSES

We also present an example of the model's utility in understanding the relative contributions of various sources to the total at-sensor radiance. Reasonable scene conditions were selected, including typical variability. A spectrally flat surface reflectance was chosen so the spectral content of the results depended only on the atmosphere and the Planck function.

Figure 2 presents the mean radiance as calculated with MODTRAN. The four components used in the FASSP model are shown: surface reflected, path scattered, surface emitted, and atmospheric emitted (upwelling) radiances. As expected, the path scattered and surface reflected dominate in the 0.4 to 2.5 μm spectral region, particularly at the lower wavelengths. In the 3 to 4 μm region, we see the cross over between the surface reflected and the surface emitted. From 4 to 14 μm , we see that the surface emitted and atmospheric emitted are comparable while the surface reflected is an order of magnitude lower.

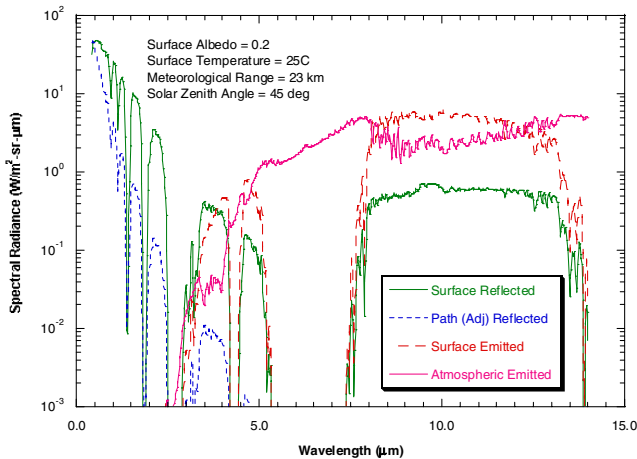


Figure 2. Example MODTRAN radiance components for sensor at 6 km.

Figure 3 plots the three surface components of the standard deviation of the at-sensor radiance. Each component was calculated by leaving that component as specified and setting the other two to zero. Below 3.5 μm , the surface reflectance variability dominates, while above 3.5 μm , the surface temperature variability dominates. Below 1 μm , the adjacent background reflectance variability contributes through the adjacency effect, but falls off rapidly at longer wavelengths.

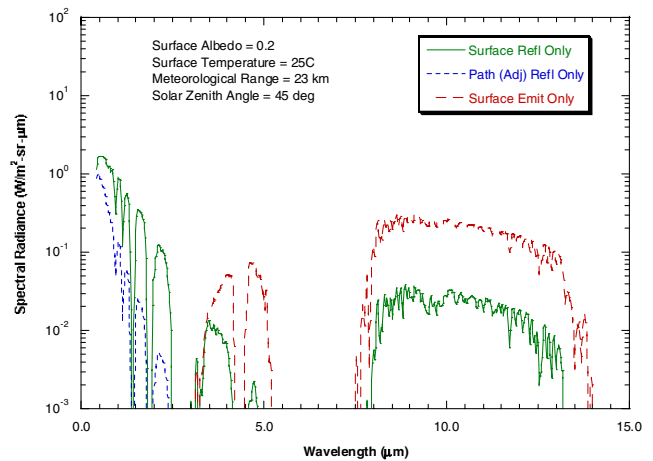


Figure 3. Example radiance standard deviations due to various components.

VI. SUMMARY AND CONCLUSIONS

Enhancements have been presented that extend the scene modeling portion of an existing hyperspectral system performance model to span the full surface remote sensing optical spectrum from 0.4 to 14 μm . The enhancements included combining the surface temperature variability with surface reflectance/emissivity variability in the upwelling radiance calculation. While these enhancements have enabled the full spectrum modeling of the scene portion of a remote sensing system, additional work remains to implement model representations of new sensors and full spectrum processing algorithms. These include algorithms for retrieving surface reflectance/emissivity and temperature. Also, additional validation efforts should be conducted as appropriate data sets become available.

VII. ACKNOWLEDGEMENTS

This work was performed while Dr. Kerekes was at MIT Lincoln Laboratory.

REFERENCES

- [1] R.O. Green, ed., "Special Issue on Imaging Spectroscopy," *Rem. Sens. of Env.*, vol. 65, no. 3, September 1998.
- [2] D. Manolakis, C. Siracusa, and G. Shaw, "Hyperspectral Subpixel Target Detection Using the Linear Mixing Model," *IEEE Trans. on Geosci. and Rem. Sens.*, vol. 39, no. 7, pp. 1392-1409, July 2001.
- [3] J.P. Kerekes and J.E. Baum, "Spectral Imaging System Analytical Model for Subpixel Object Detection," *IEEE Trans. on Geosci. and Rem. Sens.*, vol. 40, no. 5, pp. 1088-1101, May 2002.
- [4] J.P. Kerekes and D.A. Landgrebe, "An Analytical Model of Earth-Observational Remote Sensing Systems," *IEEE Trans. on Sys., Man and Cyber.*, vol. 21, no. 1, pp. 125-133, January/February, 1991.
- [5] J.P. Kerekes and J.E. Baum, "Full Spectrum Spectral Imaging System Analytical Model," accepted for publication in the *IEEE Transactions on Geoscience and Remote Sensing*, May 2004.
- [6] A. Berk, et al., "MODTRAN Cloud and Multiple Scattering Upgrades with Application to AVIRIS," *Rem. Sens. of Env.*, vol. 65, no. 3, 367-375, September 1998.
- [7] Y. J. Kaufman, "Atmospheric Effect on Spatial Resolution of Surface Imagery," *Appl. Opt.*, vol. 23, no. 19, pp. 3400-3408, 1 October 1984.
- [8] J.A. Hackwell, et al., "LWIR/MWIR Imaging Hyperspectral Sensor for Airborne and Ground-Based Remote Sensing," *Proceedings of Imaging Spectrometry II*, SPIE vol. 2819, pp. 102-107, November, 1996.